1 **Short title:** Stromule formation is causally linked to ETI signaling

2 **Author for contact:** Martin Hartmut Schattat**,** martin.schattat@pflanzenphys.uni-halle.de, +49 345 55 26286

# XopQ induced stromule formation in *Nicotiana benthamiana* is causally linked to ETI signaling and depends on ADR1 and NRG1

3 Jennifer Prautsch[a], Jessica Lee Erickson[b,c], Sedef Özyürek[a], Rahel Gormanns[a], Lars Franke[c], Jane E. Parker[e],
4 Johannes Stuttmann[b,f], Martin Hartmut Schattat[a]

5 [a]Biology, Plant Physiology, Martin-Luther-University Halle-Wittenberg, Halle, Germany

6 [b]Biology, Plant Genetics, Martin-Luther-University Halle-Wittenberg, Halle, Germany

7 [c]Leibniz-Institut for Plant Biochemistry, Halle, Germany

8 [d]Biochemistry and Biotechnology, Martin-Luther-University Halle-Wittenberg, Halle, Germany

9 [e]Max Planck Institute for Plant Breeding Research, Cologne, Germany

10 [f]Institute for Biosafety in Plant Biotechnology, Federal Research Centre for Cultivated Plants, Julius Kühn-
11 Institute (JKI), Quedlinburg, Germany

12 Author for contact: martin.schattat@pflanzenphys.uni-halle.de

13 The authors responsible for distribution of materials integral to the findings presented in this article in
14 accordance with the policy described in the Instructions for Authors (www.plantphysiol.org) is Martin Hartmut
15 Schattat (martin.schattat@pflanzenphys.uni-halle.de), Jane Parker (parker@mpipz.mpg.de) and Johannes
16 Stuttmann (jstuttmann@gmail.com).

17 One sentence summary: Genetic analysis aligns effector triggered immunity (ETI) induced stromule formation
18 with the ETI signaling cascade but not programmed cell death and questions stromule guided peri-nuclear
19 plastid clustering.

20 This study was funded by the Deutsche Forschungsgemeinschaft (DFG, German Research Foundation) –
21 400681449/GRK2498, STU642/1-1 and SFB-1403–414786233 as well as Martin-Luther-University core
22 funding.

23 Author Contributions: JLE, JS, JPa and MHS contributed to experimental design and the written text; JPr, SÖ,
24 RG and LF conducted the *A. tumefaciens* inoculation experiments in *N. benthamiana* and respective image
25 analysis; JLE conducted *Xcv* inoculation experiments and respective image analysis.

26

**Abstract**

In *Nicotiana benthamiana*, expression of the *Xanthomonas* effector XopQ triggers ROQ1-dependent ETI responses and in parallel accumulation of plastids around the nucleus and the formation of stromules. Both processes were proposed to contribute to ETI-related hypersensitive cell death and thereby to plant immunity. Whether these reactions are directly connected to ETI signaling events has not been tested. Here we utilized transient expression experiments to determine whether XopQ-mediated plastid reactions are a result of XopQ perception by ROQ1 or a consequence of XopQ virulence activity. We find that *N. benthamiana* mutants lacking ROQ1, both RNLs (NRG1 and ADR1) or EDS1, fail to elicit XopQ-dependent host cell death and stromule formation. Mutants lacking only NRG1 lost XopQ-dependent cell death but retained some stromule induction that was abolished in the RNL double mutant. This analysis aligns XopQ-induced stromules with the ETI signaling cascade but not to host programmed cell death. Furthermore, data reveal that XopQ-triggered plastid clustering is not strictly linked to stromule formation during ETI. Our data suggest that stromule formation, in contrast to chloroplast peri-nuclear dynamics, is an integral part of the *N. benthamiana* ETI response and that both RNL sub-types play a role in this ETI response.

43 **Introduction**

44 Plastids exhibit exquisite developmental flexibility, as demonstrated by their capacity to
45 differentiate into various plastid types with specialized functions, biochemical activities and
46 internal structures, depending on the plant organ, developmental stage or environmental condition.
47 Furthermore, plastids undergo extreme morphological changes, in some cases changing their shape
48 within minutes or seconds (Gunning, 2005, Pyke, 2013, Delfosse *et al.*, 2016). One highly dynamic
49 feature of plastids is the projection of long, stroma-filled tubules formed by the two envelope
50 membranes. These projections, also called stromules, are reliably observed when either the stroma
51 or the envelope membranes are fluorescently labeled (Fig. 1; reviewed in Delfosse *et al.*, 2016).
52 Over the last two decades, stromules have been detected by fluorescence microscopy in an
53 increasing number of plant species throughout the *Viridiplantae* ("green plants"; reviewed in Gray
54 *et al.*, 2001), suggesting that stromule formation emerged early during plant evolution. Examination
55 of different plant tissues revealed that while stromule frequencies may vary, stromules are a
56 ubiquitous feature of plastids (Köhler & Hanson, 2000, Holzinger *et al.*, 2008).

57 Stromules form in response to developmental cues and increase following exposure to various
58 stresses or signaling molecules and metabolites connected to stress (Schattat & Klösgen, 2011a,
59 Gray *et al.*, 2012, Mathur *et al.*, 2012, Caplan *et al.*, 2015, Vismans *et al.*, 2016), suggesting
60 stromule formation is strictly controlled by the plant. These observations led to the hypothesis that
61 stromules participate in processes that are fundamentally important for plant survival during stress,
62 to transmit signals and/or support physiological changes.

63 Despite their early emergence in the evolution of *Viridiplantae* and their frequent observation
64 across tissues, our knowledge of stromule function is limited. To date, mutants with defects in
65 signaling pathways regulating stromule formation were not identified. Therefore, it remains unclear
66 which processes or functions are carried out by stromules during stress responses and how these
67 might be executed. As an alternative to genetic dissection of stromule formation *per se*, we decided
68 instead to test effects of mutants in defined stress responses for effects on stromule formation. Our
69 aim is to gain insight into the role of stromules during adaptation to a specific stress and use genetic
70 tools to decipher stromule function.

71

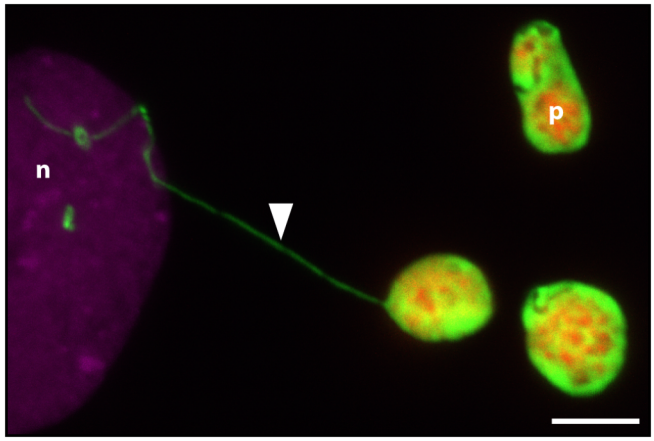


**Fig. 1: Image of a stromule connecting a plastid with a nucleus in *Nicotiana benthamiana*.** CLSM fluorescence image of an *N. benthamiana* lower leaf pavement cell expressing a nuclear marker (*H2B:mCherry* in magenta) and plastid stroma marker (*FNR:EGFP* in green); chlorophyll autofluorescence is depicted in magenta; p = plastid body, n = nucleus, arrow = stromule; scale bar corresponds to 5 µm

79 Biotic stress caused by plant interactions with recognized pathogens results in pronounced stromule
80 formation (Krenz *et al.*, 2012, Erickson *et al.*, 2014, Caplan *et al.*, 2015, Kumar *et al.*, 2018, Adlung
81 & Bonas, 2018). Many pathogenic microbes transfer virulence factors, known as effectors, into the
82 host cell cytoplasm to promote infection, often by manipulating pattern-triggered immunity (PTI)
83 programs induced by extracellular or intracellular immune receptors (Toruño *et al.*, 2016, Büttner,
84 2016). In an incompatible interaction, intracellular immune receptors recognize one or more
85 effectors. Effector recognition triggers a robust immune response termed effector-triggered
86 immunity (ETI), which frequently culminates in localized host programmed cell death (a
87 hypersensitive response = HR) at infection sites (Cui *et al.*, 2015, Yuan *et al.*, 2021). Most
88 intracellular immune receptors are nucleotide binding/leucine-rich repeat (NLR) proteins. NLR
89 proteins are represented by two major pathogen-sensing NLR receptor classes, which are defined
90 by their N/terminal domains. So called TIR-NLRs (TNLs) possess a Toll/interleukin-1 domain
91 (TIR) and CC-NLRs (CNLs) a coiled-coil (CC) domain at their N-terminus. Additionally, different
92 NLR protein families have been found to function in *A. thaliana* and Solanaceous species together
93 with pathogen-detecting (sensor) NLRs in ETI, connecting sensor NLRs with downstream
94 immunity factors and thus are called "helper" NLRs (Cui *et al.*, 2015, Wu *et al.*, 2019).

95 Dramatic increases in stromule frequencies were observed following expression of effectors
96 recognized by CC-NLRs or TIR-NLRs prior to ETI-induced cell death in *Nicotiana benthamiana*
97 and *Arabidopsis thaliana* (Caplan *et al.*, 2015, Erickson *et al.*, 2018). For example, induction of
98 ETI (resulting in HR) via the transient co-expression of the p50 helicase domain from tobacco
99 mosaic virus and the cognate TIR-NLR immune receptor, N from *Nicotiana tabacum*, in *N.*
100 *benthamiana* results in strong stromule induction (Caplan *et al.*, 2015). Similarly, a screen by our
101 group revealed that expression of XopQ from the bacterium *Xanthomonas campestris* pv.
102 *vesicatoria* (*Xcv*; strain 85-10), which is recognized by the TIR-NLR immune receptor
103 RECOGNITION OF XopQ1 (ROQ1) in *N. benthamiana*, also strongly enhanced stromule
104 frequencies (Schultink *et al.*, 2017, Erickson *et al.*, 2018). In the case of ETI activation via N/p50,
105 the authors reported that many stromules were in close proximity to the nucleus, and appeared to
106 make contact. This observation suggested that plastids might directly deliver defense signals to the
107 nucleus via stromules (Caplan *et al.*, 2015, Kumar *et al.*, 2018). Stromule frequency also increased
108 during CC-NLR and TIR-NLR mediated ETI in *Arabidopsis thaliana* when plants were challenged
109 with avirulent strains of the bacterial pathogen *Pseudomonas syringae* (Caplan *et al.*, 2015). Thus,
110 it appears that stromule formation is a common response of plants during ETI.

111 In addition to an increase in stromule frequencies and stromule-to-nucleus contacts, formation of
112 plastid clusters around nuclei was observed during ETI responses in *N. benthamiana* (Caplan *et al.*,

113 2015, Kumar *et al.*, 2018), leading to the conclusion that plastid clusters might also support delivery
114 of plastid-derived defense signals to the nucleus (Ding *et al.*, 2019, Exposito-Rodriguez *et al.*,
115 2020). In time lapse experiments spanning several minutes (Kumar *et al.*, 2018), plastid bodies
116 moved in the direction of stromule tips/anchor points in the majority of cases, giving the impression
117 that stromules directionally pull the plastid body with them. This observation led to the conclusion
118 that stromules might guide plastids to the nucleus to facilitate clustering. Hence, stromules near the
119 nucleus might have a second function in plastid positioning.

120 Taken together, ETI-induced stromules present a starting point for more detailed genetic analyses
121 of stromule formation and plastid clustering following the well-defined molecular event of effector
122 recognition. For this, we chose *N. benthamiana* ROQ1-mediated XopQ recognition leading to ETI
123 as a suitable system to critically examine the functional relationship between stromule formation
124 and immunity signaling.

125 The TNL ROQ1 was reported to oligomerize, and assemble into a tetrameric holoenzyme with
126 NADase activity (Ma *et al.*, 2020, Martin *et al.*, 2020), forming a structure similar to the pentameric
127 complex reported for the *A. thaliana* CNL ZAR1 ('resistosome'), which may directly integrate into
128 membranes to function as $Ca^{2+}$-permeable channels (Wang *et al.*, 2019a, b, Bi *et al.*, 2021). ETI
129 responses initiated by TNLs like ROQ1 require at least two more components: Heterodimeric
130 complexes composed of the lipase-like protein ENHANCED DISEASE SUSCEPTIBILITY 1
131 (EDS1) and either PHYTOALEXIN DEFICIENT4 (PAD4) or SENSECENCE ASSOCIATED
132 GENE101 (SAG101), and two types of helper NLRs, which are characterized by an N-terminal
133 four-helix bundle domain with homology to *A. thaliana* RESISTANCE to POWDERY MILDEW
134 8 (RPW8), and therefore are called RPW8-like coiled-coil ($CC_R$) domain NLRs (RNLs) (Wagner
135 *et al.*, 2013, Jubic *et al.*, 2019, Castel *et al.*, 2019, Wu *et al.*, 2019, Gantner *et al.*, 2019, Lapin *et*
136 *al.*, 2019, Saile *et al.*, 2020).

137 Molecular functions of EDS1 yet remain elusive, but its heterodimeric complexes are essential for
138 TNL-mediated immune responses in different dicot plants including *A. thaliana* and *N.*
139 *benthamiana* (Wagner *et al.*, 2013, Gantner *et al.*, 2019, Lapin *et al.*, 2020). There are two types of
140 RNLs known ACTIVATED DISEASE RESISTANCE GENE 1 (ADR1) and N REQUIREMENT
141 GENE 1 (NRG1) and members of both types can be found in *A. thaliana* and *N. benthamiana*
142 (Collier *et al.*, 2011, Lapin *et al.*, 2020). In *A. thaliana*, distinct EDS1-PAD4-ADR1 and EDS1-
143 SAG101-NRG1 modules appear to regulate pathogen resistance and cell death, respectively, in
144 TNL immunity (Lapin *et al.*, 2019, Sun *et al.*, 2020). In contrast, immune functions are not known
145 for *Nb*EDS1-*Nb*PAD4 in *N. benthamiana*, and an *Nb*EDS1-*Nb*SAG101b complex appears to

146 operate mainly through *Nb*NRG1 to mediate both cell death and resistance in this species (Qi *et al.*,
147 2018, Gantner *et al.*, 2019, Lapin *et al.*, 2019). *Nb*ADR1 immune functions were so far not
148 analyzed, but *Nb_nrg1* mutant plants, but not *Nb_eds1* mutant plants, still mobilize significant
149 XopQ/Roq1-mediated transcriptional reprogramming, despite a loss of resistance and absence of
150 cell death, thus suggesting some degree of cooperativity or redundancy between the two helper
151 NLR classes also in *N. benthamiana* TNL immunity (Qi *et al.*, 2018, Saile *et al.*, 2020).

152 In this study, we capitalized on the previous characterization of XopQ/ROQ1-induced TNL
153 immunity in *N. benthamiana* and positioned chloroplast stromule formation and perinuclear
154 clustering in downstream signaling networks. Our data suggest that, although stromule formation
155 is tightly linked to immune responses, it can be uncoupled from ETI-triggered cell death.
156 Furthermore, our data support partially redundant functions of the NRG1 and ADR1 helper NLRs
157 (hNLRs) in stromule formation. Intriguingly, our data indicate that plastid clustering can be
158 largely uncoupled from ROQ1 ETI and hence is unlikely to represent an integral component of
159 the plant innate immune response.

160 **Results**

161 ***Xcv*-mediated stromule formation in *N. benthamiana* depends on XopQ**

162 We previously reported that *A. tumefaciens* mediated transient expression of XopQ from *Xcv*
163 induces stromule formation in *N. benthamiana* (Erickson *et al.*, 2018). During infection with *Xcv*
164 strains such as *Xcv* 85-10, a strain which naturally delivers XopQ to host cells, XopQ is likely less
165 abundant in infected cells than during transient expression experiments. Additionally, XopQ is
166 translocated together with the entire type III-secreted effectome of *Xcv* (> 30 effectors; Teper *et al.*,
167 2016). In order to test the extent to which stromule frequencies measured during transient
168 expression experiments reflect the *Xcv* interaction, different bacterial strains were inoculated into
169 *FNR:eGFP* expressing transgenic *N. benthamiana* plants. Under our greenhouse conditions the
170 wild-type strain *Xcv* 85-10 induces an ETI-associated programmed cell death response (indicating
171 XopQ recognition), showing first signs of dead leaf tissue at 2 dpi (Adlung *et al.*, 2016). In order
172 to be able to observe plastids in living cells, we collected leaf samples for microscopy 43 hours
173 post-inoculation (hpi) (Fig. 2A). To test the role XopQ and other effectors play in stromule
174 response, *Xcv* mutant strains *ΔhrcN* and *ΔxopQ* were infiltrated on the same leaf with the wild-type
175 strain. The *ΔhrcN* mutant is deficient in typeIII secretion and serves as a non-virulent PTI control
176 (Lorenz & Büttner, 2009). *ΔhrcN* as well as *ΔxopQ* mutant strains of *Xcv* did not induce
177 macroscopically visual changes in infected tissues at 2 dpi and were not distinguishable from the

178 mock infiltration (Fig. 2A; Lorenz & Büttner, 2009, Adlung *et al.*, 2016, Adlung & Bonas, 2017).
179 When analyzing the stromule phenotype, treatments differed significantly: The *Xcv* 85-10 strain
180 induced massive stromule induction in the infiltrated tissue. The *ΔxopQ* and *ΔharcN* (no effector
181 translation) mutant-inoculated tissue harbored almost no stromules, with levels comparable to mock
182 inoculations (10 mM $MgCl_2$) and *ΔhrcN*, which does not translocate any effectors (Fig. 2B,
183 Supplemental materials Table S1).

184 Together with transient expression experiments using *A. tumefaciens* (Erickson et al., 2018), these
185 results indicate that stromule induction at 2 dpi by the wild-type strain is strictly dependent on
186 presence of XopQ. No other effectors in this strain contributed measurably to stromule induction
187 at 2 dpi, when translocated at natural levels. In conclusion, inoculations with *Xcv* strains show that
188 XopQ-triggered stromules appear during pathogen attack at 2 dpi, and supports the idea that
189 stromule induction during transient assays recapitulates a physiologically relevant phenotype.

190

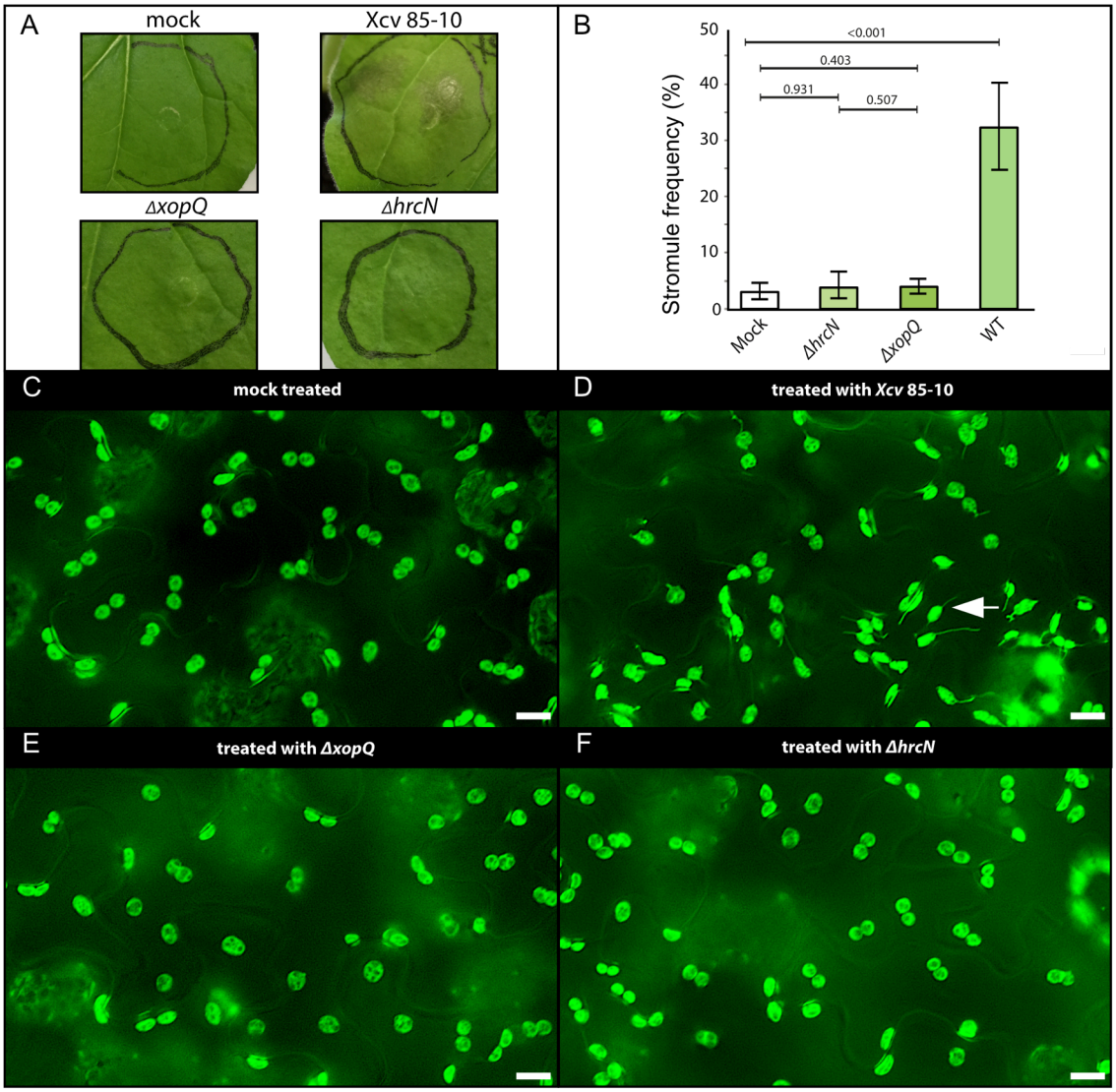


**Fig. 2: *Xanthomonas campestris pv. vesicatoria* (*Xcv*) inoculation experiments in wild-type *FNR:eGFP* transgenic plants.** (**A**) Macroscopic phenotypes of leaves infiltrated with different Xcv strains at 2 dpi.(**B**) Stromule frequency (SF%) of *Xcv*-inoculated tissue at 43 hpi. Bars in the bar plot represent arithmetic averages (three repeats with 5 plants each); error bars represent 95% confidence intervals; p-values of statistical tests are shown above the black lines; (**C - F**) Sample sectors of representative microscopic images used for stromule quantification. Green fluorescence originates from the stably expressed *FNR:eGFP* plastid stroma marker; scale bars = 10 µm; arrow = stromule. (full-frame images Supplemental materials Fig. S1 and S2)

201 **XopQ fails to induce high stromule frequency values in *roq1* mutant plants**

202 We next examined the extent to which XopQ-mediated stromule induction in the lower epidermis
203 of *N. benthamiana* is a consequence of XopQ perception by TNL receptor ROQ1, using *A.*
204 *tumefaciens*-based transient gene expression. Different *N. benthamiana* mutant lines impaired in
205 XopQ perception or lacking TNL downstream signaling components were co-infiltrated with
206 Agrobacterium strains for expression of stroma-targeted eGFP (*SSU:eGFP*) and either
207 *xopQ:mOrange2* or *mOrange2* alone, as control. Agrobacterium strains were infiltrated at a final
208 $OD_{600} = 0.2$, which led to only moderate Agrobacterium-dependent stromule induction (< 20 %,
209 Erickson *et al.*, 2014) well below XopQ-induced stromule frequencies (~ 60 %). These
210 experimental conditions were evaluated using *N. benthamiana* stably expressing stromal-targeted
211 eGFP (*FNR:eGFP*; Supplemental materials Fig. S3).

212 We first tested XopQ-mediated stromule frequencies in *roq1* mutant plants (*roq1-3* and *-4*). ROQ1-
213 deficient plants fail to recognize XopQ and therefore lack the typical ETI-induced yellowing and
214 chlorosis exhibited by wild-type plants following transient XopQ expression (Schultink *et al.*, 2017;
215 Gantner *et al.*, 2019). *xopQ:mOrange2* or the *mOrange2* control were co-infiltrated with a stroma-
216 targeted GFP (*ssu:eGFP*) into wild-type and mutant plants to allow for the visualization of plastids
217 and stromules. As a control for XopQ recognition, macroscopic phenotypes of the co-infiltrated
218 leaves were recorded 10 dpi, a time point when symptoms are clear despite the low optical densities
219 used for infiltration resulted (Fig. 3A). As expected, *xopQ:mOrange2* expression in wild-type
220 plants resulted in chlorosis of the infiltration spot, indicative of the XopQ-induced ETI response
221 (Adlung *et al.*, 2016). In *roq1-3* and *roq1-4* plants, there was no visible chlorosis and tissues were
222 indistinguishable from control infiltrations. In all plant lines, *mOrange2* controls showed stromule
223 frequency values characteristic for leaves infiltrated with „empty“ GV3101 (pMP90) bacteria
224 (compare Fig. 3B with Supplemental materials Fig. S3), indicating that the *roq1* mutation does not
225 increase basal stromule frequencies. *xopQ:mOrange2* expression resulted in significantly higher
226 stromule induction in wild-type plants, as previously described (Erickson et al., 2018). In contrast,
227 *xopQ:mOrange2* expression failed to induce stromules beyond GV3101 (pMP90) basal levels in
228 the *roq1-3* and *roq1-4* mutant plants (Fig. 3B; Supplemental materials Table S2). Average stromule
229 frequencies in mutants infiltrated with *xopQ:mOrange2* were equal to or less than mORANGE2
230 controls. Fig. 3C, D and f show representative microscopy images of *xopQ:mOrange2* expressing
231 tissues. The full loss of XopQ-induced stromule formation in *roq1* mutant plants shows that XopQ
232 recognition by ROQ1 is required for stromule induction, and that non-recognized XopQ activity
233 does not generate a stromule-inducing signal.

234

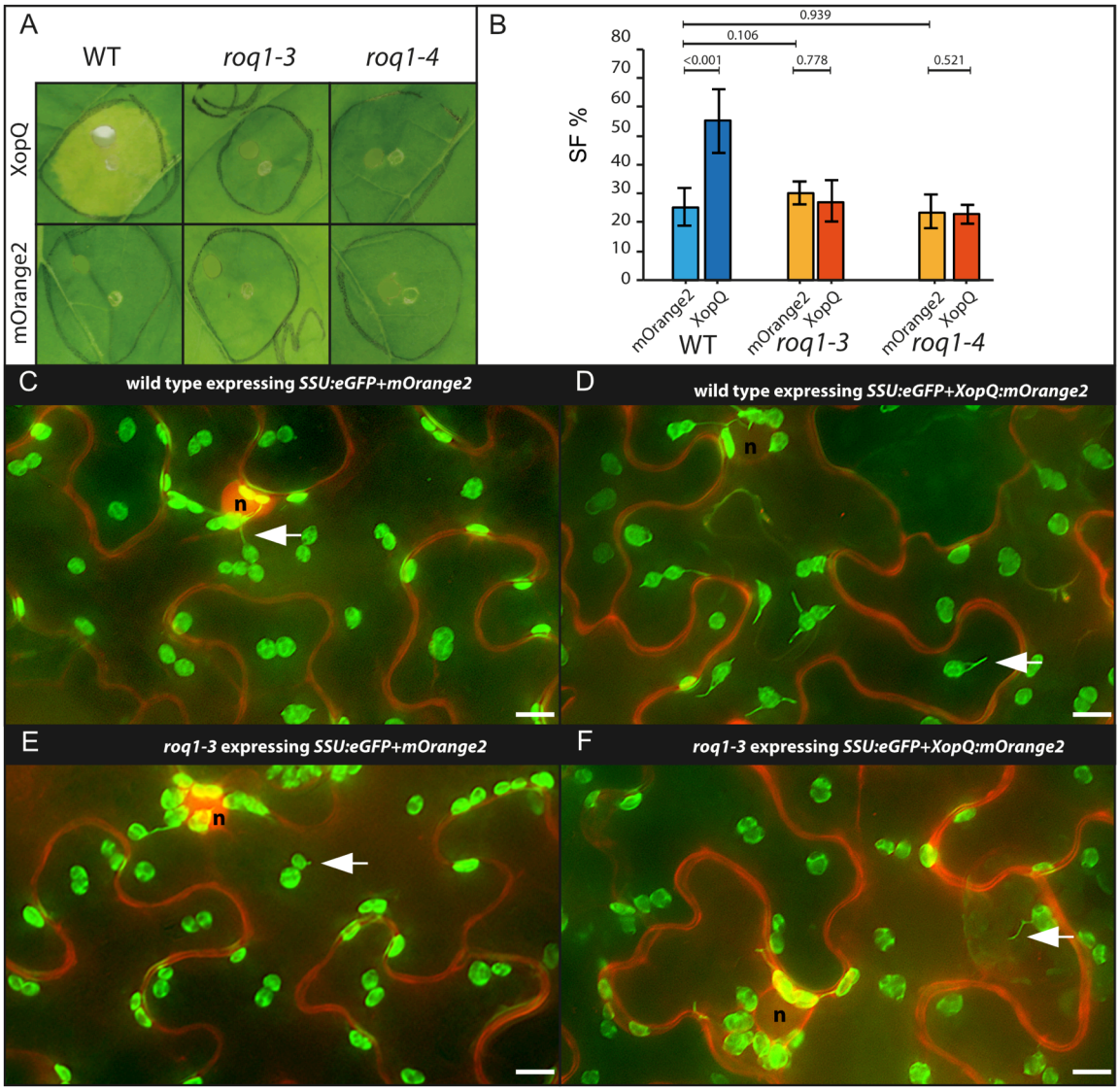


**Fig. 3: Test for XopQ mediated stromule formation in lower leaf epidermis cells of *roq1* mutants (*Nicotiana benthamiana*).** (**A**) Macroscopic phenotypes of Agrobacterium-mediated *xopQ:mOrange2* and *mOrange2*-expression in wildtype, *roq1-3* and *roq1-4* leaves 10 dpi. (**B**) Results of stromule quantification expressed as stromule frequency (SF%). Bars in the bar plot represent arithmetic averages; error bars represent 95% confidence intervals; p-values of the statistical tests are shown above the black lines. (**C - F**) Sample sectors of representative microscopic images used for stromule quantification. Green fluorescence originates from the SSU:eGFP plastid stroma marker; red fluorescence originates from the mORANGE2 fluorescence protein (c and e = *mOrange2* controls; d and f *mOrange2* fused to *xopQ*); nuclei = "n"; arrow = stromule; scale bars = 10 µm. (full-frame images Supplemental materials Fig. S4 and Fig. S5)

248 **XopQ/ROQ1-dependent stromule induction requires EDS1**

249 EDS1 is essential for resistance and cell death mediated by TNL-type immune receptor ROQ1
250 (Adlung *et al.*, 2016, Gantner *et al.*, 2019). In order to test if XopQ-mediated stromule formation
251 is dependent on EDS1, mixed infiltrations were repeated in *eds1a-1* knockout and wild-type plants.
252 In respect to stromule frequency and macroscopic phenotype the wildtype plants responded as seen
253 in previous experiments (Fig. 4A and B; Supplemental materials Table S2). In contrast to the
254 wildtype *eds1a-1* plants did not show signs of chlorosis at 10 dpi in response to *xopQ:mOrange2*
255 expression, which is consistent with literature reports (Fig. 4A; Adlung *et al.*, 2016, Gantner *et al.*,
256 2019). As was the case for *roq1* mutant plants, XopQ-induced stromules were not observed in
257 *eds1a-1* tissues (Fig. 4B and F; Supplemental materials Table S2). These results indicate that
258 stromule formation in response to XopQ occurs downstream of EDS1 signaling, suggesting that
259 XopQ-ROQ1 interaction and ROQ1 tetramerization ('resistosome' formation; Schultink *et al.*,
260 2017, Martin *et al.*, 2020) are not sufficient to induce stromules.

261

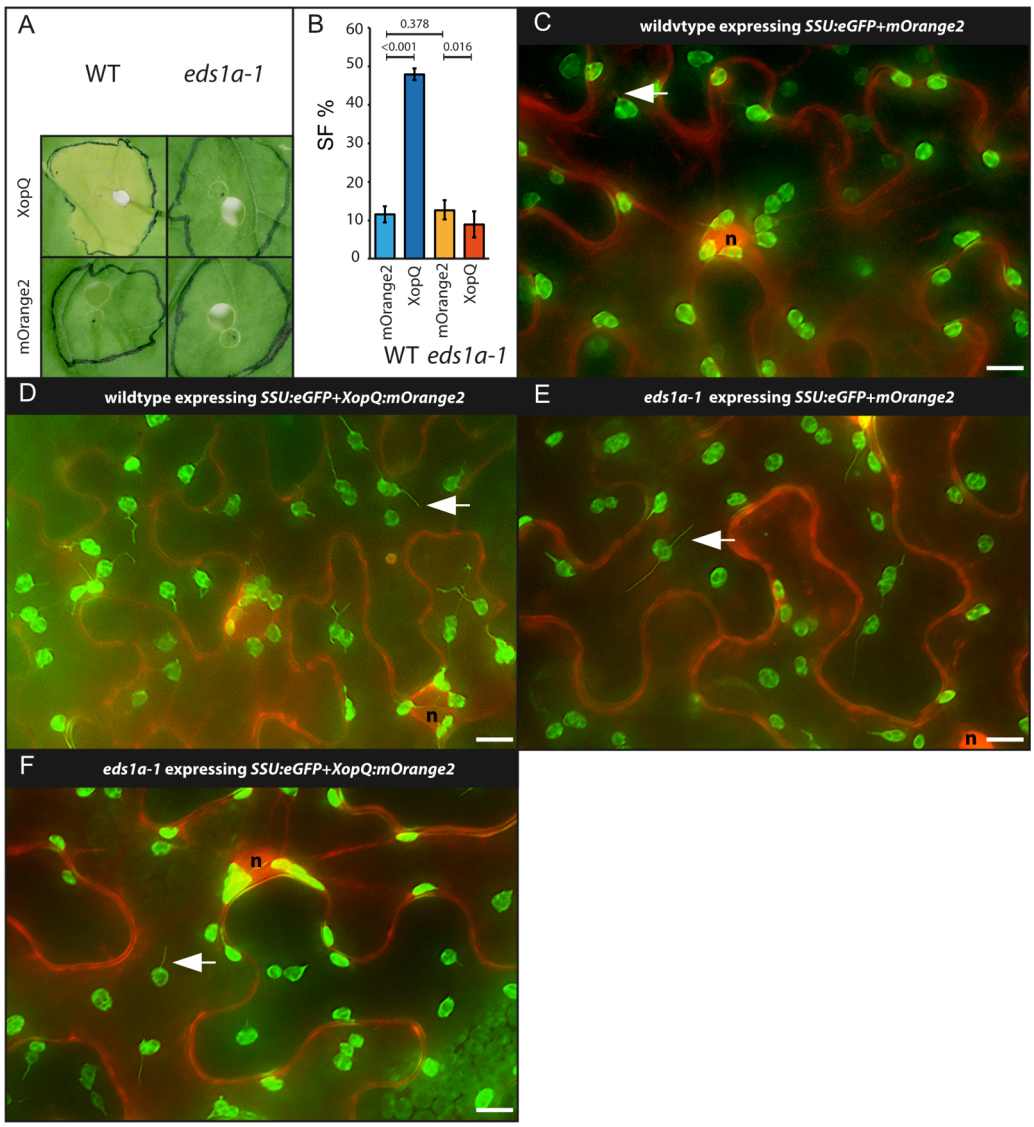


262

263 **Fig. 4: Test for XopQ-mediated stromule formation in the lower leaf epidermis of *eds1a-1***
264 **mutants (*Nicotiana benthamiana*).** (**A**) Macroscopic phenotypes of *xopQ:mOrange2* and
265 *mOrange2* infiltrated wildtype and *eds1a-1* leaves 10 dpi. (**B**) Results of stromule quantification
266 expressed as stromule frequency (SF%). Bars in the bar plot represent arithmetic averages (three
267 repeats with 5 plants each); error bars represent 95% confidence intervals; p-values of the
268 statistical tests are shown above the black lines; (**C - F**) sample sectors of representative
269 microscopic images from the data set used for stromule quantification. Green fluorescence
270 originates from the SSU:eGFP plastid stroma marker; red fluorescence originates from the
271 mORANGE2 fluorescence protein (c and e untagged mOrange2; d and f mOrange2 fused to
272 XopQ); nuclei = "n"; arrow = stromule; scale bars = 10 µm. (full-frame images Supplemental
273 materials Fig. S6.)

274

275 **XopQ-induced stromule induction depends on RNL activity but is not a consequence of host**
276 **cell death**

277 In *A. thaliana*, RNL-type NLRs of the ADR1 and NRG1 subfamilies contribute to TNL immunity
278 (Castel *et al.*, 2019, Wu *et al.*, 2019, Lapin *et al.*, 2019, Saile *et al.*, 2020). In *N. benthamiana nrg1*
279 mutant plants, resistance and cell death induced by several TNLs was fully abolished, suggesting
280 NRG1 as the major RNL in TNL immunity in this species (Qi *et al.*, 2018). To test if XopQ-
281 stimulated stromule formation is NRG1-dependent, two mutant lines with different genomic
282 deletions, *nrg1-4* and *nrg1-5* (Ordon *et al.*, 2021) were analyzed. The *nrg1* mutants did not show
283 signs of yellowing in response to *A. tumefaciens* mediated XopQ expression, and infiltration spots
284 were macroscopically indistinguishable from control infiltrations (Fig. 5A), as expected (Qi *et al.*,
285 2018, Ordon *et al.*, 2021). All three plant lines responded similarly to the *mOrange2* control
286 expression, with stromule frequencies reaching approximately 25 % (Fig. 5B; Supplemental
287 materials Table S2). In contrast, the response to *xopQ*:*mOrange2* was markedly different between
288 wild-type and *nrg1* mutant lines (Fig. 5B). *xopQ*:*mOrange2* expression in the *nrg1* background
289 induced stromule frequencies values, which were between Agrobacterium-inoculated and
290 x*opQ*:*mOrange2* -inoculated wild-type plants. Although *roq1*, *eds1* and *nrg1* mutants were equally
291 deficient in XopQ-induced cell death (necrosis), stromule formation did not strictly require NRG1,
292 and is thus uncoupled from cell death in *Nb_nrg1* mutant plants.

293 So far, a function of ADR1 was not identified in *N. benthamiana* (Lapin et al., 2019, Sun et al.,
294 2021) but varied contributions of these RNLs to Arabidopsis TNL ETI suggested that *N.*
295 *benthamiana* ADR1 might steer residual stromule formation in *N. benthamiana nrg1* lines.
296 Therefore, we tested stromule formation in response to XopQ in a newly generated *Nbadr1_nrg1*
297 double mutant line using mixed infiltrations as before. As in the *nrg1* single mutants,
298 *xopQ:mOrange2* expression did not induce yellowing or cell death in *adr1_nrg1* plants (Fig. 6A).
299 In contrast to our observations in *nrg1* single mutants, *xopQ:mOrange2* did not induce the
300 formation of stromules beyond the mORANGE2 control (Fig. 6B; Supplemental materials Table
301 S2). Accordingly, the *adr1_nrg1* mutant exhibited stromule and cell death phenotypes similar to
302 the *roq1* (Fig. 3A) and *eds1* (Fig. 4A) mutant lines. Overall, these results show that not only NRG1
303 but also ADR1 contributes to stromule formation in *N. benthamiana*. Hence, these results uncover
304 that the ADR1-family of RNLs exhibits not only ETI signaling functions in *A. thaliana* ETI but
305 also functions in the ETI response of solanaceous plants.

306

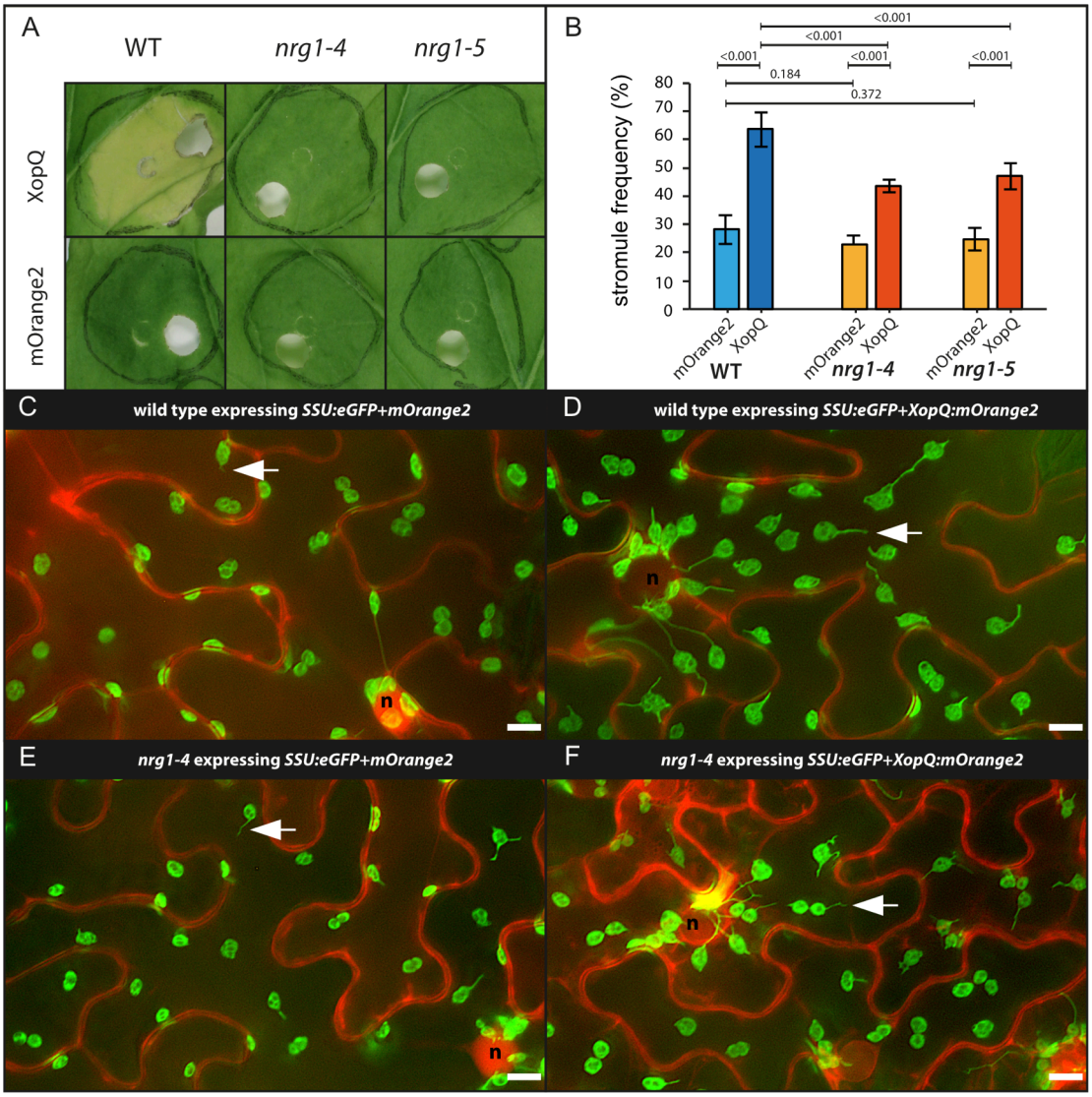


**Fig. 5: Test for XopQ mediated stromule formation in lower leaf epidermis cells of *nrg1* mutants (*Nicotiana benthamiana*).** (**A**) Macroscopic phenotypes of *XopQ:mOrange2* and *mOrange2*-infiltrated wildtype, *nrg1-4* and *nrg1-5* leaves at 10 dpi.(**B**) Results of stromule quantification expressed as stromule frequency (SF%). Bars in the bar plot represent arithmetic averages (three repeats with 5 plants each); error bars represent 95% confidence intervals; p-values of the statistical tests are shown above the black lines. (**C - F**) Sample sectors of representative microscopic images used for stromule quantification. Green fluorescence originates from the SSU:eGFP plastid stroma marker; red fluorescence originates from the mORANGE2 fluorescence protein (c and e = *mOrange2* control; d and f = *mOrange2* fused to *XopQ*); nuclei = "n"; arrow = stromule; scale bars = 10 µm. (full-frame images in Supplemental materials Fig. S7).

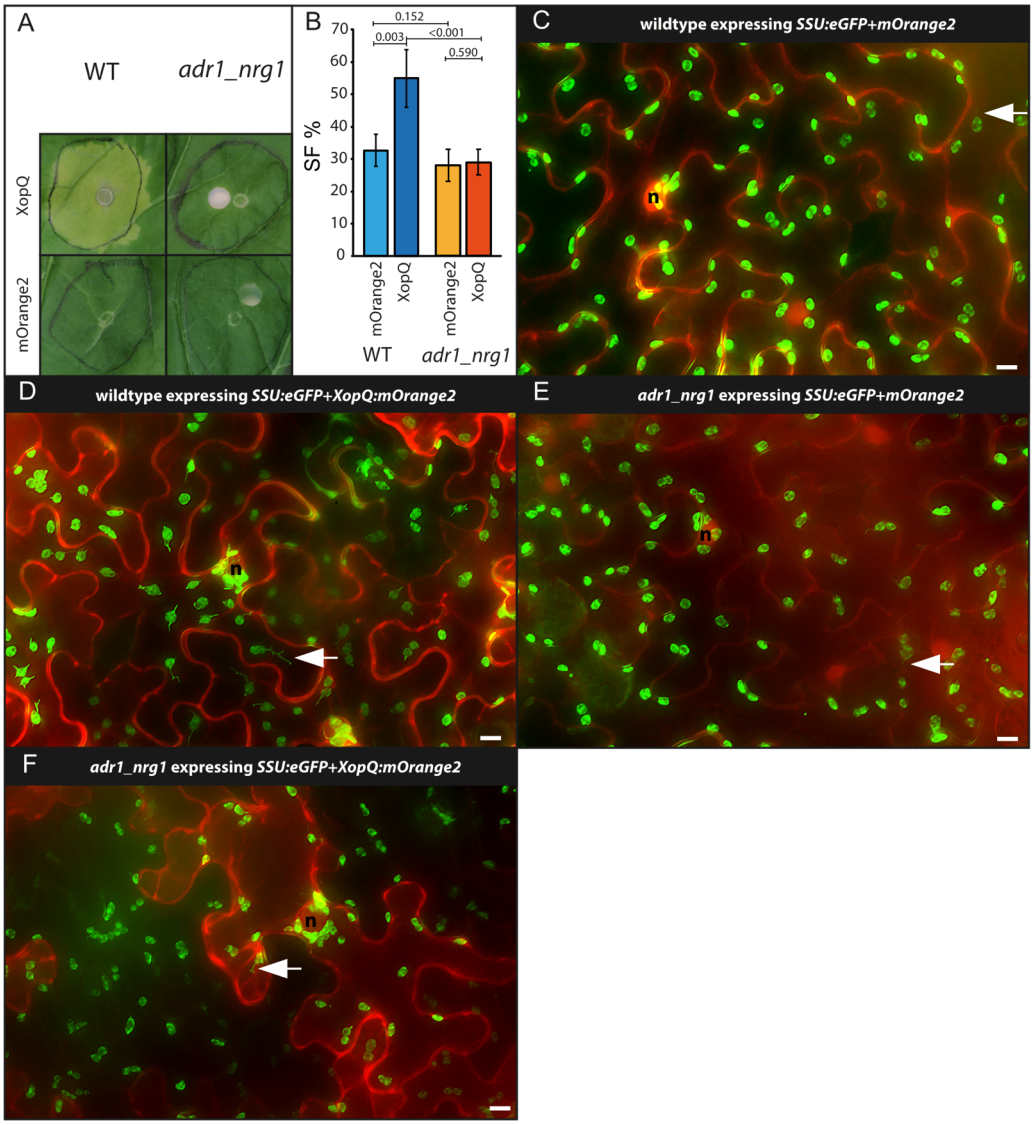


**Fig. 6: Test for XopQ mediated stromule formation in lower leaf epidermis cells of adr1_nrg1 double mutants (*Nicotiana benthamiana*).** (**A**) Macroscopic phenotypes of *xopQ:mOrange2* and *mOrange2*-infiltrated wildtype and *adr1_nrg1-5* leaves at 10 dpi. (**B**) Results of stromule quantification expressed as stromule frequency (SF%). Bars in the bar plot represent arithmetic averages; error bars represent 95% confidence intervals; p-values of the statistical tests are shown above black lines; wild-type 3 plants and *adr1_nrg1* 5 plants for each of 3 repeats. (**C - F**) Cropped images used for stromule quantification. Green fluorescence originates from the SSU:eGFP plastid stroma marker; red fluorescence originates from the mORANGE2 fluorescence protein (c and e are *mOrange2* controls; d and f show *mOrange2* translation fusion with *XopQ*); nuclei = "n"; arrow = stromule; scale bars = 10 µm. (full-frame images shown in Supplemental materials Fig. S8).

332 **XopQ-induced peri-nuclear plastid clustering does not require TNL immune signaling**

333 In order to test if XopQ-induced ETI facilitates formation of chloroplast clusters, and whether this
334 has the same genetic dependencies as found for stromule frequency, chloroplast clustering was
335 quantified in wild-type, *roq1-3*, *eds1a-1*, *nrg1-4* and *adr1_nrg1* lines. As a measure for plastid
336 clustering, the number of plastids in close proximity (up to one plastid in diameter) to the nucleus
337 was counted and expressed as the plastid nucleus association index (PNAI, see Erickson *et al.*,
338 2014, 2018). In these experiments, mORANGE2 or XopQ:mORANGE2 fluorescence,
339 respectively, served to highlight the position of nuclei (see Fig. 7B - K). In control infiltrations
340 (*mOrange2*), wild-type and all four mutants produced similar numbers of plastids around the
341 nucleus (Fig. 7A; Supplemental materials Table S3). No significant differences in PNAI were
342 detected. When challenged with XopQ, plastid clustering increased in wild-type plants (Fig. 7A;
343 Supplemental materials Table S3). Although plastid clustering has been considered an ETI response
344 (Caplan *et al.*, 2015, Kumar *et al.*, 2018, Ding *et al.*, 2019), we found that XopQ-induced plastid
345 clustering was not diminished in mutant lines impaired in XopQ recognition or downstream
346 signaling (Fig. 7A; Supplemental materials Table S3). Upon expression of *xopQ:mOrange2, nrg1-*
347 *4* showed wild-type levels of plastid clustering, while *roq1-3*, *eds1* and *adr1_nrg1* mutants had
348 significantly higher PNAI values (Fig. 7A; Supplemental materials Table S3). Fig. 7B - K shows
349 representative images of the different plant lines expressing *ssu:eGFP+xopQ:mOrange2* or
350 *ssu:eGFP+mOrange2*.

351 We concluded that when the XopQ-induced ETI signal cascade is blocked (*roq1, eds1* and
352 *adr1_nrg1* mutants), the tendency of plastids to cluster around the nucleus remains, and is even
353 enhanced compared to wild-type or plants (*nrg1* mutant) with partially intact signaling (Fig. 7H).
354 These data suggest that one feature of ROQ1/XopQ-induced ETI is suppression of plastid
355 clustering.

356

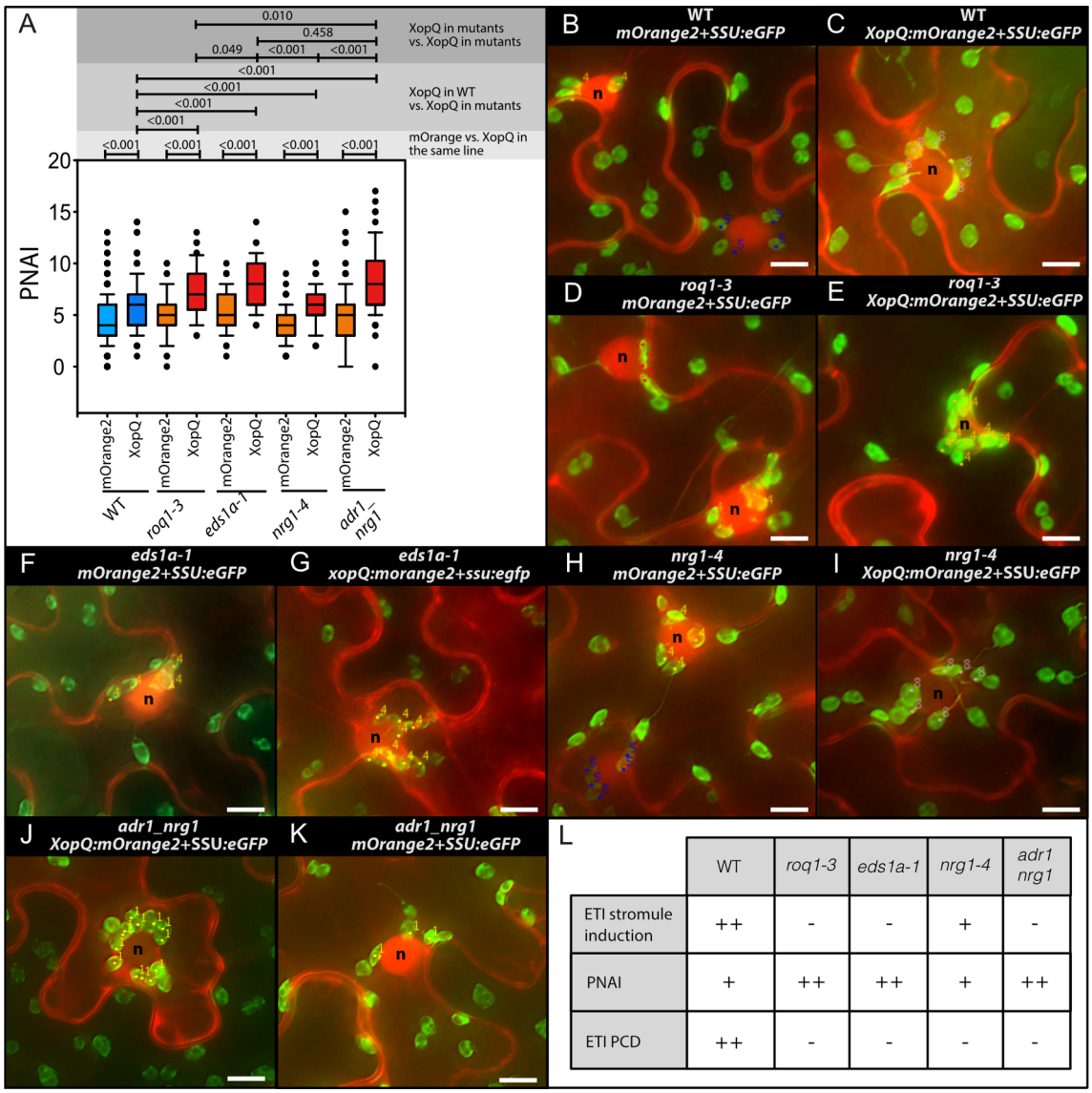


| | WT | roq1-3 | eds1a-1 | nrg1-4 | adr1 nrg1 |
|---|---|---|---|---|---|
| ETI stromule induction | ++ | - | - | + | - |
| PNAI | + | ++ | ++ | + | ++ |
| ETI PCD | ++ | - | - | - | - |

**Fig. 7: PNAI - Analysis of plastid clustering in response to XopQ expression (*Nicotiana benthamiana*).** Plastid nucleus association index (PNAI) at 3 dpi following *mOrange2* and *xopQ:mOrange2* expression in wild/type as well as mutant plant lines (*roq1-3*, *eds1a*, *nrg1-4* and *adr1_nrg1*). (**A**) PNAI values represented in box plots (box line = median, whiskers = 10$^{th}$ as well as 90$^{th}$ percentile, with each outlier plotted); p-values of Mann-Whitney rank sum tests are shown above the lines in grey boxes. (**B - K**) Sample images of nuclei with associated plastids (labeled with a dot a number as they were during original plastid scoring); "n" = nuclei; scale bars = 10 µm. (**L**) Summary of observed ETI stromule, PNAI and cell death phenotypes where "-" = no change compared to control, "+" = visible but moderate increase in cell death; "++" = strong increase.

368 **Discussion**

369 Here, we set out to understand how ETI-associated stromule formation aligns with signaling
370 processes downstream of immune receptor activation, using recognition of the effector XopQ by
371 the TNL ROQ1 in *N. benthamiana* as a case study. A quantitative analysis of stromule formation
372 and peri-nuclear plastid clustering in XopQ recognition and ETI signaling mutants produced several
373 important insights. First, complete absence of a XopQ-related stromule response in *roq1* and *eds1*
374 mutants shows that XopQ-induced stromules are not a result of its virulence/effector activity, but
375 result from effector recognition by the ROQ1 immune receptor and a resulting *EDS1*-dependent
376 ETI response. Second, residual induction of stromules in the *nrg1* mutant in the absence of
377 appreciable cell death suggests that induced stromule formation is not a consequence of ETI-related
378 host cell death but more closely related to pathogen resistance. Third, analysis of the *nrg1_adr1*
379 double mutant line reveals that residual XopQ-induced ETI and stromule frequency in *nrg1* (but
380 not *eds1*), is conferred by ADR1 in *N. benthamiana*. This reveals an ADR1 contribution to TNL
381 ETI processes in a solanaceous plant, suggesting usage of both RNLs NRG1 and ADR1 branches
382 in ETI, as observed in Arabidopsis. Finally, ROQ1/XopQ-induced plastid clustering does not
383 correlate with ETI induction and stromule formation and is thus likely to be a direct or indirect
384 consequence of XopQ virulence activity during infection. A model summarizing these findings is
385 presented in Fig. 8A and B.

386 **Uncoupling immune signaling and HR-induced stromules**

387 Stromules have been proposed to transmit retrograde signals to the nucleus, and amplify
388 programmed cell death responses as part of ETI (Caplan *et al.*, 2015). More recently it was
389 suggested that stromules have the added function of locating and pulling plastid bodies to the
390 nucleus (Kumar *et al.*, 2018). So far, all reported microbial effectors that induce stromules also
391 provoked programmed cell death (Caplan et al., 2015, Erickson et al., 2018). Therefore, it remained
392 unclear whether stromule formation accompanies the cascade of events contributing to host cell
393 death or is a by-product of physiological changes in cells as they die. The observed stromule
394 induction upon XopQ expression in *nrg1* mutant plants without cell death or measurable resistance
395 (Qi *et al.*, 2018) (Fig. 5A) suggests stromules represent events upstream of ETI-related pathogen
396 resistance and host cell death. Hence, ETI-induced stromule formation is not coupled to cellular
397 destruction but more likely an integral part of the ETI response, as suggested previously (Caplan *et*
398 *al.*, 2015).

399 **ADR1 contributes to TNL immunity and stromule formation in *N. benthamiana***

400 Dicot genomes encoding TNL receptors generally also encode RNL-type NLRs of the ADR1 and
401 NRG1 classes (Collier *et al.*, 2011, Lapin *et al.*, 2020). In *A. thaliana*, both classes of RNLs
402 contribute to immunity to different extents. Three *A. thaliana* ADR1 paralogs have functions in
403 basal immunity to virulent pathogens related to salicylic acid, and they also contribute to PTI
404 (Bonardi *et al.*, 2011, Jubic *et al.*, 2019, Pruitt *et al.*, 2021, Tian *et al.*, 2021). ADR1s and NRG1s
405 contribute to different extents to *A. thaliana* TNL immunity, and function as distinct modules,
406 respectively with EDS1-PAD4 and EDS1-SAG101 dimers regulating pathogen resistance and cell
407 death (Lapin et al., 2019, Saile et al., 2020, Lapin et al., 2020, Sun et al., 2021). In *N. benthamiana*,
408 only EDS1-SAG101 appeared to execute TNL ETI, and NRG1 was identified as a major RNL
409 required for cell death and resistance mediated by several tested TNLs (Qi *et al.*, 2018 , Gantner *et*
410 *al.*, 2019). A role for *N. benthamiana* ADR1 in immunity was so far not detected, although Qi et
411 al. (2018) reported residual transcriptional reprogramming occurring upon ROQ1 activation in
412 *nrg1*, but not *eds1* mutant plants. Notably, *NbADR1* was among the upregulated genes of an *NRG1*-
413 independent regulon (Qi et al, 2018). Residual stromule formation in *nrg1*, but not *eds1* or
414 *nrg1_adr1* (compare panel '(A)' in Supplemental materials Fig. S4, 5 and 6) supports an *Nb*ADR1
415 contribution to TNL-ETI in *N. benthamiana*. Hence, stromule formation appears to be a highly
416 sensitive read-out for ETI induction, occurring in the absence of cell death or measurable pathogen
417 resistance which are blocked in *N. benthamiana nrg1* and *eds1* mutants (Qi et al 2018). Current
418 evidence suggests that, besides the sensor CNL ZAR1, RNLs also might assemble into pore-
419 forming resistosome complexes and function as $Ca^{2+}$ permeable cation channels (Wang *et al.*,
420 2019a, Jacob *et al.*, 2021, Bi *et al.*, 2021). Induced $Ca^{2+}$influx into host cells would then amplify
421 ROS generation and salycilic acid signaling as well as transcription (Lu and Tsuda 2021, Yuan *et*
422 *al.*, 2021). In future work, it will be interesting to examine whether $Ca^{2+}$ levels inside cells influence
423 stromule formation, as stromule-to-nucleus connections were found to contribute to ROS formation
424 (Caplan *et al.*, 2015).

425 **Is perinuclear plastid clustering independent of ETI stromule induction?**

426 In an emerging concept, plastids are the source of important immune response signaling and defense
427 metabolites, including precursors of salicylic acid and jasmonic acid. Many plastid-derived signals
428 must reach the nucleus to fulfill their proposed functions (reviewed in Kretschmer *et al.*, 2020).
429 Thus, re-localization of plastids towards the nucleus might promote more efficient signal
430 transmission. Indeed, when challenged with different pathogens and $H_2O_2$, plastids relocated
431 towards the nucleus in *N. benthamiana* epidermis leaf cells, forming peri-nuclear clusters (Erickson
432 *et al.*, 2014, Caplan *et al.*, 2015, Ding *et al.*, 2019a). How plant cells regulate re-localization of
433 plastids to the nucleus upon different stimuli remains unknown. Based on observations of stromule

434 orientation often coinciding with plastid directional movement, it was proposed that stromules are
435 initiated during ETI and extended along the microtubules network, finding anchor points on actin
436 filaments close to the nucleus which guide plastid body movement towards nuclei (Kumar *et al.*,
437 2018). Peri-nuclear plastid clustering, as a consequence, might enhance plastid-to-nucleus signal
438 transfer underpinning immune responses. When we challenged wild-type plants with
439 *XopQ:mOrange2*, stromule formation as well as perinuclear plastid clustering were consistently
440 induced in lower epidermis cells (Fig. 7A -K). Additionally, stromules facing the nucleus and
441 seemingly anchored in the nuclear periphery were observed (see Fig.s 3B, 4B, 5B and 6B for SF%;
442 e.g. 3D, 4D and 5D for nucleus-associated stromules). Both observations support stromules guiding
443 plastid body movement (Kumar et al., 2018). However, based on this model we expected impaired
444 or abolished perinuclear clustering in plant lines unable to recognize XopQ (*roq1*) or to initiate
445 TNL immunity (*eds1*, *nrg1*, *nrg1_adr1*). Despite, having reduced numbers of ETI-associated
446 stromules, the plastid clustering still occurred when *XopQ:mOrange2* was expressed in respective
447 mutant backgrounds. Notably, plastid clustering was more pronounced in the mutants compared to
448 wild type. In contrast, perinuclear clustering in response to *XopQ:mOrange2* expression was not
449 slightly reduced in *nrg1* plants (Fig. 7 A-K). In summary, we observe a negative correlation
450 between stromule frequency and perinuclear plastid clustering. Accordingly, in our assays ETI
451 induction of stromules was associated with lower plastid clustering compared to when ETI was
452 disabled (Fig. 7H). These data suggest that increased chloroplast guidance towards the nucleus via
453 stromules does not facilitate ETI but might be due to XopQ virulence activity.

454 **Is induction of peri-nuclear plastid clustering a part of XopQ's function?**

455 Stronger plastid clustering observed in the absence of ROQ1, EDS1, ADR1_NRG1 suggests it
456 may represent a consequence of undisturbed XopQ activity (Fig. 7A and 8B). This observation
457 partially contradicts the suggestion that peri-nuclear plastid clustering supports ETI responses by
458 facilitating more efficient transfer of pro-defense signals from plastids to the nucleus (discussed
459 in Exposito-Rodriguez et al., 2020). If the sole function of peri-nuclear plastids is to enhance ETI,
460 why should the bacteria facilitate peri-nuclear plastid clustering via XopQ in the absence of
461 effector recognition? Conversely, why suppress clustering when ETI is induced by XopQ? Our
462 results suggest that clustering may serve multiple functions or is the consequence of several
463 stimuli in plant pathogen interactions. In support of this hypothesis while plastid clustering in *N.*
464 *benthamiana* occurs in response to ETI triggering stimuli (e.g. TMV-p50 and RPS2 recognition
465 Kumar *et al.*, 2018, Ding et al., 2019), it also occurs in response to pattern triggered immunity
466 (PTI) stimuli (*Pst* DC3000 *ΔhopQ1-1*, flg22 and $H_2O_2$, Ding et al., 2019), which demonstrates
467 that plastid clustering is not ETI specific. Additionally, plastid clustering is not restricted to plant

468 microbe interactions and has been found to be important for plastid inheritance during cell
469 division (Sheahan et al., 2004 and 2020) and has been observed following the exposure of *N.*
470 *benthamiana* epidermis leaf cells to cytokinin (Erickson et al., 2014). In summary, although
471 plastid accumulation at the nucleus is linked to plant microbe interactions it is not exclusively so,
472 and may reflect one output resulting from changes to different cell physiological parameters (i.e.,
473 altered hormone or $H_2O_2$ levels). Currently, although we see that XopQ activity induces
474 clustering, the trigger for this phenotype remains enigmatic and it remains to be seen whether it is
475 of any benefit to *Xcv* during an infection.

476 **Conclusion**

477 We set out in this study to test two hypotheses about stromule function in the context of effector
478 triggered immunity. We provide here experimental evidence for a direct link for ETI-induced
479 stromule formation, supporting the hypothesis of Caplan et al. (2015), which suggests that
480 stromules play a specific role during ETI. Our findings therefore encourage the enquiry of the
481 nature of this specific role in future. In contrast to this, our results do not support the second
482 hypothesis, which suggested that stromules might be needed to guide plastid movement towards
483 the nucleus (Kumar et al., 2018), highlighting the fact that there is currently no mechanistic
484 explanation for peri-nuclear plastid accumulation and that for this phenomenon fundamental work
485 still has to be done. Finally, the obtained results in the *nrg1* and *adr1_nrg1* mutants (cooperative
486 activity of NRG1 and ADR1 in ETI signaling) show the potential of stromules to function as a
487 quantifiable and sensitive readout for branches of ETI signaling, which result in currently used
488 assays only in hard to detect differences.

489

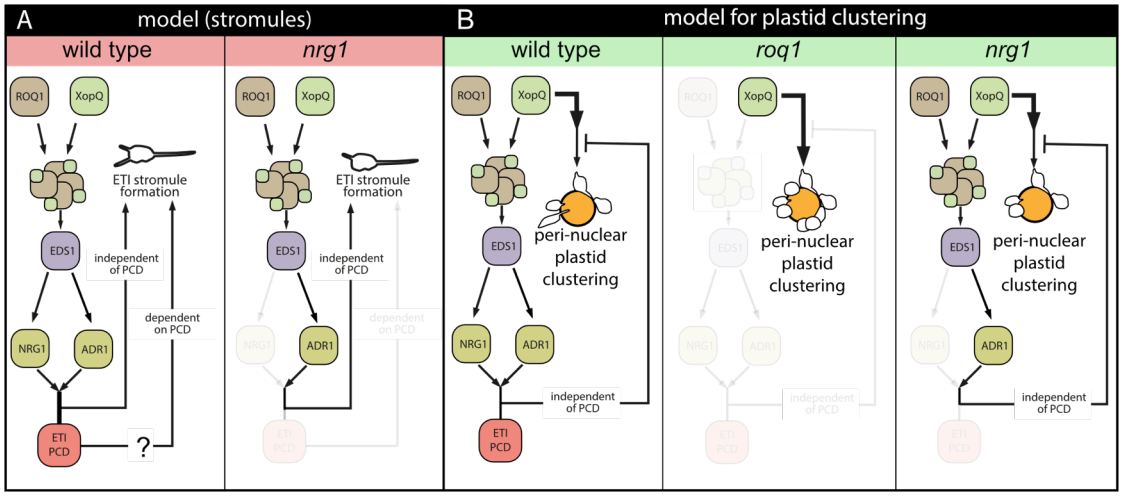


490

491 **Fig. 8: Model of XopQ mediated stromule induction and peri-nuclear plastid clustering. (A)**
492 Model for effector triggered immunity (ETI) induced stromule formation by XopQ in wild-type
493 plants (left panel): XopQ (*Xanthomonas outer protein Q*) is recognized by the TIR-NB-LRR
494 (TOLL INTERLEUKIN 1 RECEPTOR NUCLEOTIDE BINDING LEUCIN RICH REPEAT)
495 resistance protein ROQ1 (RECOCNITION OF XopQ 1), which forms with XopQ a heteromeric
496 protein complex, the so called 'resistosome'. From the 'resistosome' the information of XopQ
497 recognition is transferred with the help of EDS1 (ENHANCED DISEASE SUSCEPTIBILITY 1)
498 to the RNL class helper NLRs NRG1 and ADR1, which culminates in PCD (programmed cell
499 death) as well as stromule formation. In *nrg1* mutants (right panel) XopQ fails to induce cell death
500 but at the same time still shows significant ETI stromule induction mediated by ADR1. This
501 indicates the existence of a PCD independent ETI stromule induction pathway. However, at this
502 point a role for PCD in stromule induction, or a role for stromules in PCD is not ruled out (?). **(B)**
503 Model for peri-nuclear plastid clustering following *xopQ* expression: In wildtype plants (left) an
504 intact ETI signal chain partially suppresses the strong peri-nuclear plastid clustering induced by
505 XopQ presence. When ETI signal transduction is blocked (*eds1*, *roq1* and *adr_nrg1* mutants) this
506 suppression does not take place and plastid clustering is enhanced (middle). The restricted ETI
507 signal chain in *nrg1* mutants (right) is sufficient for suppression of induced peri-nuclear plastid
508 clustering to wildtype levels, thus suppressing signals likely originate from this pathway. Both
509 models only consider genes, which were analyzed as part of this study. The role of the different
510 proteins forming distinct complexes with EDS1 will have to be elucidated in future.

511

512 **Material and Methods**

513 **Plant material**

514 *Nicotiana benthamiana* plant lines used in this study were: wild type, *roq1-3* and *roq1-4* (Gantner
515 *et al.*, 2019), *eds1-1* (also referred to as *eds1a-1*; Ordon *et al.*, 2017), *nrg1-4* and *nrg1-5* (Ordon *et*
516 *al.*, 2021). An *adr1_nrg1* double mutant was created by genome editing using a derivative of
517 pDGE311, a plant transformation vector containing additional counter-selection markers and an
518 intron-optimized *zCas9i* gene, as recently described (Grützner *et al.*, 2021, Stuttmann *et al.*, 2021)
519 (Methods S1). For *Xanthomonas* inoculations transgenic *N. benthamiana* plants of the plant line
520 FNR:eGFP#7-25 expressing the plastid marker FNR:eGFP (Schattat et al., 2011b) were used.
521 Plants were grown in long day conditions (16h day and 8h night) in green house chambers with
522 controlled temperature and humidity. Temperature was approximately 23 °C during the day and
523 19 °C at night. Relative humidity was kept around 55 %.

524 **Bacterial strains and cultivation**

525 *E. coli* Top10 cells were used for cloning and DNA propagation. Cells were cultivated at 37 °C in
526 LB with the appropriate antibiotic selection. Agrobacterium strain GV3101 (pMP90) (Koncz &
527 Schell, 1986) was grown in liquid or on solid YEB media containing rifampicin, gentamycin and
528 either spectinomycin or carbenicillin, while *Xcv* strains were grown in NYG medium
529 supplemented with rifampicin (30 °C for both). *Xanthomonas* strains utilized were: *Xcv* 85-10
530 (wild-type; Thieme *et al.*, 2005), *Xcv ΔhrcN* (strain deficient in an ATPase required for typeIII
531 secretion of effectors; Lorenz & Büttner, 2009 and *Xcv ΔxopQ* Adlung *et al.*, 2016).

532 **Plasmids**

533 For visualization of plastids and stromules a plastid organelle marker construct was created using
534 the Modular Cloning Toolbox (Weber *et al.*, 2011, Engler *et al.*, 2014). The final construct
535 consisted of the *35S* promotor (pICH51277), the chloroplast transit peptide of RUBISCO (pAGS-
536 L0-#115 in backbone pICH41258), eGFP (pAGS-L0-#050 backbone pICH41264) and the NOS
537 terminator (pICH41421), assembled in an Level 1 acceptor plasmid. The *XopQ:mOrange2*
538 expression construct was described previously (Erickson et al., 2018; for more details see
539 Methods S2).

540 ***Agrobacterium tumefaciens*-mediated transient expression**

541 Plasmids were transformed into *A. tumefaciens* strain GV3101 (pMP90). For transient expression
542 experiments, strains harboring the binary vectors were grown overnight in 5 ml YEB liquid
543 cultures (with appropriate antibiotics), harvested by centrifugation and resuspended in
544 agrobacterium infiltration medium (10 mM $MgCl_2$; 5 mM MES pH 5.6; 0.15 µM
545 Acetosyringone) with a final optical density ($OD_{600nm}$) of 0.2. Bacteria harboring the plastid
546 marker and the effector or the mORANGE2 control were mixed in a 1:1 ratio. Using a needless
547 syringe, bacterial suspensions were inoculated into intercostal areas of the youngest fully
548 expanded leaves of 5–6-week-old *N. benthamiana* plants (see Methods S3).

549 ***Xanthomonas campestris pv. vesicatoria* inoculations**

550 *Xcv* NYG liquid cultures were centrifuged to harvest cells, bacteria was resuspended in 10 mM
551 $MgCl_2$, and suspensions adjusted to an $OD_{600nm}$ of 0.1. All three strains, as well as a buffer
552 control, were then inoculated as described for *A. tumefaciens*. Plastids/stromules were observed at
553 2 days post-infiltration (dpi) using an epi-fluorescence microscope.

554 **Imaging hardware**

555 For image acquisition, an epi-fluorescence microscope (AxioObserver Z1) setup from Zeiss
556 (Jena, Germany) equipped with an X-Cite fluorescence light source and a MRm monochrome
557 camera (Zeiss, Jena, Germany) was used. GFP fluorescence was recorded using a 38 HE filter
558 cube (Carl Zeiss AG, Jena, Germany). mORANGE2 fluorescence was recorded utilizing the 43
559 HE filter cube (Carl Zeiss AG. Jena, Germany). The microscope manufacturer's software
560 (ZenBlue, Zeiss, Germany) controlled image acquisition. All images were captured using a 40x /
561 0.75 NA EC PLAN NEOFLUAR lens.

562 **Imaging procedures and image processing**

563 For quantification of stromule frequencies, a single leaf disc of each infiltration spot was
564 harvested using a cork borer. Leaf discs were vacuum-infiltrated, mounted on glass slides and
565 three independent z-stacks of the lower epidermis were collected in transmitted light, eGFP and
566 mORANGE2 channels. In order to obtain 2D extended depth of field images for quantification,
567 single images of the z-series of each channel were first exported into separate file folders and
568 subsequently combined into single images using software and procedures described in Schattat &
569 Klösgen, 2009 (total of 3 images per disc).

570 For quantification of stromule frequencies (SF%) we measured the proportion of plastids with at
571 least one stromule (Erickson et al., 2014). To facilitate the faster quantification of stromule and
572 plastid counts in *N. benthamiana* tissues, we expanded on the previously published
573 MTBCellCounter (Franke *et al.*, 2015) via a ridge detection-based stromule detection algorithm
574 (Möller & Schattat, 2019). The extended MTBCellCounter allows for the detection of plastid
575 bodies as described in Franke *et al.*, 2015 and identifies subsequently plastids with stromules.

576 The plastid nucleus association index (PNAI) was described previously (Erickson *et al.*, 2014),
577 and represents the absolute number of plastids in close association with a given nucleus. PNAI
578 was evaluated in the 2D projected images (see image processing). Nuclei were counted as nucleus
579 associated when either the plastid body touched, overlapped with, or was within a distance of
580 4µm from the nucleus. 4µm corresponds to the average epidermis plastid diameter.

581 For sample sizes and details on statistical analysis of SF% and PNAI see Supplemental materials
582 Methods S4 Notes S1.

583 **Naming conventions**

584 For conventions used to name mutants, genes, proteins and artificial DNA constructs see Methods
585 S5.

586 **Acknowledgments**

587 All *Xcv* strains were kindly provided by Prof. Ulla Bonas, Martin-Luther-Universität Halle-
588 Wittenberg, Germany. Dr. Sebastian Schornack, TSL, Cambridge, UK for advice on the
589 manuscript. This study was funded by the Deutsche Forschungsgemeinschaft (DFG, German
590 Research Foundation) – 400681449/GRK2498, STU642/1-1 and SFB-1403–414786233 as well
591 as Martin-Luther-University core funding.

592

593 **References**


594 **Adlung N, Bonas U** (2017) Dissecting virulence function from recognition: cell
595 death suppression in Nicotiana benthamiana by XopQ/HopQ1-family effectors relies on
596 EDS1-dependent immunity. Plant J **91**: 430–442

597 **Adlung N, Prochaska H, Thieme S, Banik A, Blüher D, John P, Nagel O, Schulze S, Gantner**
598 **J, Delker C, et al** (2016) Non-host Resistance Induced by the Xanthomonas Effector XopQ
599 Is Widespread within the Genus Nicotiana and Functionally Depends on EDS1. Front Plant
600 Sci **7**: 1796

601 **Bi G, Su M, Li N, Liang Y, Dang S, Xu J, Hu M, Wang J, Zou M, Deng Y, et al** (2021) The
602 ZAR1 resistosome is a calcium-permeable channel triggering plant immune signaling. Cell
603 **184**: 3528–3541.e12

604 **Bonardi V, Tang S, Stallmann A, Roberts M, Cherkis K, Dangl JL** (2011) Expanded
605 functions for a family of plant intracellular immune receptors beyond specific recognition of
606 pathogen effectors. Proceedings of the National Academy of Sciences **108**: 16463–16468

607 **Büttner D** (2016) Behind the lines–actions of bacterial type III effector proteins in plant cells.
608 FEMS Microbiology Reviews **40**: 894–937

609 **Caplan JL, Kumar AS, Park E, Padmanabhan MS, Hoban K, Modla S, Czymmek K,**
610 **Dinesh-Kumar SP** (2015) Chloroplast Stromules Function during Innate Immunity.
611 Developmental Cell **34**: 45–57

612 **Castel B, Ngou P-M, Cevik V, Redkar A, Kim D-S, Yang Y, Ding P, Jones JDG** (2019)
613 Diverse NLR immune receptors activate defence via the RPW8-NLR NRG1. New
614 Phytologist **222**: 966–980

615 **Collier SM, Hamel L-P, Moffett P** (2011) Cell death mediated by the N-terminal domains of a
616 unique and highly conserved class of NB-LRR protein. MPMI **24**: 918–931

617 **Cui H, Tsuda K, Parker JE** (2015) Effector-triggered immunity: from pathogen perception to
618 robust defense. Annu Rev Plant Biol **66**: 487–511

619 **Delfosse K, Wozny MR, Jaipargas E-A, Barton KA, Anderson C, Mathur J** (2016)
620 Fluorescent Protein Aided Insights on Plastids and their Extensions: A Critical Appraisal.
621 Front Plant Sci. doi: 10.3389/fpls.2015.01253

**Ding X, Jimenez-Gongora T, Krenz B, Lozano-Duran R** (2019) Chloroplast clustering around the nucleus is a general response to pathogen perception in Nicotiana benthamiana. Mol Plant Pathol **8**: 521

**Engler C, Youles M, Gruetzner R, Ehnert T-M, Werner S, Jones JDG, Patron NJ, Marillonnet S** (2014) A golden gate modular cloning toolbox for plants. ACS Synth Biol **3**: 839–843

**Erickson JL, Adlung N, Lampe C, Bonas U, Schattat MH** (2018) The Xanthomonas effector XopL uncovers the role of microtubules in stromule extension and dynamics in Nicotiana benthamiana. Plant J **93**: 856–870

**Erickson JL, Ziegler J, Guevara D, Abel S, Klösgen RB, Mathur J, Rothstein SJ, Schattat MH** (2014) Agrobacterium-derived cytokinin influences plastid morphology and starch accumulation in Nicotiana benthamiana during transient assays. BMC Plant Biol **14**: 127–120

**Franke L, Erickson JL, Rödel D, Schröter D, Storbeck B, Möller B, Schattat MH** (2015) The "MTB Cell Counter" a versatile tool for the semi-automated quantification of sub-cellular phenotypes in fluorescence microscopy images. A case study on plastids, nuclei and peroxisomes. **26**: 031–042

**Gantner J, Ordon J, Kretschmer C, Guerois R, Stuttmann J** (2019) An EDS1-SAG101 Complex Is Essential for TNL-Mediated Immunity in Nicotiana benthamiana. The Plant Cell **31**: 2456–2474

**Gray JC, Hansen MR, Shaw DJ, Graham K, Dale R, Smallman P, Natesan SKA, Newell CA** (2012) Plastid stromules are induced by stress treatments acting through abscisic acid. Plant J **69**: 387–398

**Gray JC, Sullivan JA, Hibberd JM, Hansen MR** (2001) Stromules: Mobile protrusions and interconnections between plastids. Plant Biology **3**: 223–233

**Grützner R, Martin P, Horn C, Mortensen S, Cram EJ, Lee-Parsons CWT, Stuttmann J, Marillonnet S** (2021) High-efficiency genome editing in plants mediated by a Cas9 gene containing multiple introns. Plant Communications **2**: 100135

**Gunning BES** (2005) Plastid stromules: video microscopy of their outgrowth, retraction, tensioning, anchoring, branching, bridging, and tip-shedding. Protoplasma **225**: 33–42

651 **Holzinger A, Kwok EY, Hanson MR** (2008) Effects of arc3, arc5 and arc6 mutations on plastid
652 morphology and stromule formation in green and nongreen tissues of Arabidopsis thaliana.
653 Photochem Photobiol **84**: 1324–1335

654 **Jacob P, Kim NH, Wu F, Kasmi El F, Chi Y, Walton WG, Furzer OJ, Lietzan AD, Sunil S,**
655 **Kempthorn K, et al** (2021) Plant "helper" immune receptors are Ca2+-permeable
656 nonselective cation channels. Science (New York, NY) **373**: 420–425

657 **Jubic LM, Saile S, Furzer OJ, Kasmi El F, Dangl JL** (2019) Help wanted: helper NLRs and
658 plant immune responses. Current Opinion in Plant Biology **50**: 82–94

659 **Koncz C, Schell J** (1986) The promoter of T L-DNA gene 5 controls the tissue-specific
660 expression of chimaeric genes carried by a novel type of Agrobacterium binary vector. **204**:
661 383–396

662 **Köhler RH, Hanson MR** (2000) Plastid tubules of higher plants are tissue-specific and
663 developmentally regulated. Journal of Cell Science **113 ( Pt 1)**: 81–89

664 **Krenz B, Jeske H, Kleinow T** (2012) The induction of stromule formation by a plant DNA-virus
665 in epidermal leaf tissues suggests a novel intra- and intercellular macromolecular trafficking
666 route. Front Plant Sci **3**: 291

667 **Kretschmer M, Damoo D, Djamei A, Kronstad J** (2020) Chloroplasts and Plant Immunity:
668 Where Are the Fungal Effectors? Pathogens 2020, Vol 9, Page 19 **9**: 19

669 **Kumar AS, Park E, Nedo A, Alqarni A, Ren L, Hoban K, Modla S, McDonald JH,**
670 **Kambhamettu C, Dinesh-Kumar SP, et al** (2018) Stromule extension along microtubules
671 coordinated with actin-mediated anchoring guides perinuclear chloroplast movement during
672 innate immunity. Elife. doi: 10.7554/eLife.23625

673 **Lapin D, Bhandari DD, Parker JE** (2020) Origins and Immunity Networking Functions of
674 EDS1 Family Proteins. Annu Rev Phytopathol **58**: 253–276

675 **Lapin D, Kovacova V, Sun X, Dongus JA, Bhandari D, Born von P, Bautor J, Guarneri N,**
676 **Rzemieniewski J, Stuttmann J, et al** (2019) A Coevolved EDS1-SAG101-NRG1 Module
677 Mediates Cell Death Signaling by TIR-Domain Immune Receptors. The Plant Cell **31**: 2430–
678 2455

**Lorenz C, Büttner D** (2009) Functional characterization of the type III secretion ATPase HrcN from the plant pathogen Xanthomonas campestris pv. vesicatoria. J Bacteriol **191**: 1414–1428

**Lu Y, Tsuda K** (2021) Intimate Association of PRR- and NLR-Mediated Signaling in Plant Immunity. MPMI **34**: 3–14

**Ma S, Lapin D, Liu L, Sun Y, Song W, Zhang X, Logemann E, Yu D, Wang J, Jirschitzka J, et al** (2020) Direct pathogen-induced assembly of an NLR immune receptor complex to form a holoenzyme. Science (New York, NY). doi: 10.1126/science.abe3069

**Martin R, Qi T, Zhang H, Liu F, King M, Toth C, Nogales E, Staskawicz BJ** (2020) Structure of the activated ROQ1 resistosome directly recognizing the pathogen effector XopQ. Science (New York, NY). doi: 10.1126/science.abd9993

**Mathur J, Mammone A, Barton KA** (2012) Organelle extensions in plant cells. Journal of Integrative Plant Biology **54**: 851–867

**Möller B, Schattat MH, 2019, 2019** Quantification of Stromule Frequencies in Microscope Images of Plastids Combining Ridge Detection and Geometric Criteria. pdfs.semanticscholar.org

**Mullineaux PM, Selga T, Selga M, Exposito-Rodriguez M, Laissue PP, Gobiņš V, Smirnoff N, Laser AO, 2010, Park E** (2020) Spatial chloroplast-to-nucleus signalling involving plastid-nuclear complexes and stromules. Philos Trans R Soc Lond B Biol Sci **375**: 20190405

**Ordon J, Gantner J, Kemna J, Schwalgun L, Reschke M, Streubel J, Boch J, Stuttmann J** (2017) Generation of chromosomal deletions in dicotyledonous plants employing a user-friendly genome editing toolkit. Plant J **89**: 155–168

**Ordon J, Martin P, Erickson JL, Ferik F, Balcke G, Bonas U, Stuttmann J** (2021) Disentangling cause and consequence: genetic dissection of the DANGEROUS MIX2 risk locus, and activation of the DM2h NLR in autoimmunity. Plant J **106**: 1008–1023

**Pruitt RN, Locci F, Wanke F, Zhang L, Saile SC, Joe A, Karelina D, Hua C, Fröhlich K, Wan W-L, et al** (2021) The EDS1-PAD4-ADR1 node mediates Arabidopsis pattern-triggered immunity. Nature 1985 313:6005 **598**: 495–499

**Pyke KA** (2013) Divide and shape: an endosymbiont in action. Planta **237**: 381–387

**Qi T, Seong K, Thomazella DPT, Kim JR, Pham J, Seo E, Cho M-J, Schultink A, Staskawicz BJ** (2018) NRG1 functions downstream of EDS1 to regulate TIR-NLR-mediated plant immunity in Nicotiana benthamiana. Proc Natl Acad Sci USA **115**: E10979–E10987

**Saile SC, Jacob P, Castel B, Jubic LM, Salas-Gonzáles I, Bäcker M, Jones JDG, Dangl JL, Kasmi El F** (2020) Two unequally redundant "helper" immune receptor families mediate Arabidopsis thaliana intracellular “sensor” immune receptor functions. PLOS Biology **18**: e3000783

**Schattat M, Barton K, Baudisch B, Klösgen RB, Mathur J** (2011) Plastid stromule branching coincides with contiguous endoplasmic reticulum dynamics. Plant Physiol **155**: 1667–1677

**Schattat MH, Klösgen RB** (2009) Improvement of plant cell microscope images by use of “depth of field-”extending software. Endocytobiosis and Cell Research 11–19

**Schattat MH, Klösgen RB** (2011) Induction of stromule formation by extracellular sucrose and glucose in epidermal leaf tissue of Arabidopsis thaliana. BMC Plant Biol **11**: 115

**Schultink A, Qi T, Lee A, Steinbrenner AD, Staskawicz B** (2017) Roq1 mediates recognition of the Xanthomonas and Pseudomonas effector proteins XopQ and HopQ1. Plant J **92**: 787–795

**Sheahan MB, Collings DA, Rose RJ, McCurdy DW** (2020) ACTIN7 Is Required for Perinuclear Clustering of Chloroplasts during Arabidopsis Protoplast Culture. Plants 2020, Vol 9, Page 225 **9**: 225

**Sheahan MB, Rose RJ, McCurdy DW** (2004) Organelle inheritance in plant cell division: the actin cytoskeleton is required for unbiased inheritance of chloroplasts, mitochondria and endoplasmic reticulum in dividing protoplasts. Plant J **37**: 379–390

**Stuttmann J, Barthel K, Martin P, Ordon J, Erickson JL, Herr R, Ferik F, Kretschmer C, Berner T, Keilwagen J, et al** (2021) Highly efficient multiplex editing: one-shot generation of 8× Nicotiana benthamiana and 12× Arabidopsis mutants. Plant J **106**: 8–22

**Sun X, Lapin D, Feehan JM, Stolze SC, Kramer K, Dongus JA, Rzemieniewski J, Blanvillain-Baufumé S, Harzen A, Bautor J, et al** (2021) Pathogen effector recognition-dependent association of NRG1 with EDS1 and SAG101 in TNL receptor immunity. Nature Communications **12**: 3335–15

**Sun Y, Zhu Y-X, Balint-Kurti PJ, Wang G-F** (2020) Fine-Tuning Immunity: Players and Regulators for Plant NLRs. Trends in Plant Science **25**: 695–713

**Teper D, Burstein D, Salomon D, Gershovitz M, Pupko T, Sessa G** (2016) Identification of novel Xanthomonas euvesicatoria type III effector proteins by a machine-learning approach. Mol Plant Pathol **17**: 398–411

**Thieme F, Koebnik R, Bekel T, Berger C, Boch J, Büttner D, Caldana C, Gaigalat L, Goesmann A, Kay S, et al** (2005) Insights into genome plasticity and pathogenicity of the plant pathogenic bacterium Xanthomonas campestris pv. vesicatoria revealed by the complete genome sequence. J Bacteriol **187**: 7254–7266

**Tian H, Wu Z, Chen S, Ao K, Huang W, Yaghmaiean H, Sun T, Xu F, Zhang Y, Wang S, et al** (2021) Activation of TIR signalling boosts pattern-triggered immunity. Nature 1985 313:6005 **598**: 500–+

**Toruño TY, Stergiopoulos I, Coaker G** (2016) Plant-Pathogen Effectors: Cellular Probes Interfering with Plant Defenses in Spatial and Temporal Manners. Annu Rev Phytopathol **54**: 419–441

**Vismans G, van der Meer T, Langevoort O, Schreuder M, Bouwmeester H, Peisker H, Dörman P, Ketelaar T, van der Krol A** (2016) Low-Phosphate Induction of Plastidal Stromules Is Dependent on Strigolactones But Not on the Canonical Strigolactone Signaling Component MAX2. Plant Physiol **172**: 2235–2244

**Wagner S, Stuttmann J, Rietz S, Guerois R, Brunstein E, Bautor J, Niefind K, Parker JE** (2013) Structural basis for signaling by exclusive EDS1 heteromeric complexes with SAG101 or PAD4 in plant innate immunity. Cell Host Microbe **14**: 619–630

**Wang J, Hu M, Wang J, Qi J, Han Z, Wang G, Qi Y, Wang H-W, Zhou J-M, Chai J** (2019a) Reconstitution and structure of a plant NLR resistosome conferring immunity. Science (New York, NY). doi: 10.1126/science.aav5870

**Wang J, Wang J, Hu M, Wu S, Qi J, Wang G, Han Z, Qi Y, Gao N, Wang H-W, et al** (2019b) Ligand-triggered allosteric ADP release primes a plant NLR complex. Science (New York, NY). doi: 10.1126/science.aav5868

**Weber E, Engler C, Gruetzner R, Werner S, Marillonnet S** (2011) A Modular Cloning System for Standardized Assembly of Multigene Constructs. PLoS ONE **6**: e16765

767 **Wu Z, Li M, Dong OX, Xia S, Liang W, Bao Y, Wasteneys G, Li X** (2019) Differential
768 regulation of TNL-mediated immune signaling by redundant helper CNLs. New Phytologist
769 **222**: 938–953

770 **Yuan M, Ngou BPM, Ding P, Xin X-F** (2021) PTI-ETI crosstalk: an integrative view of plant
771 immunity. Curr Opin Plant Biol **62**: 102030